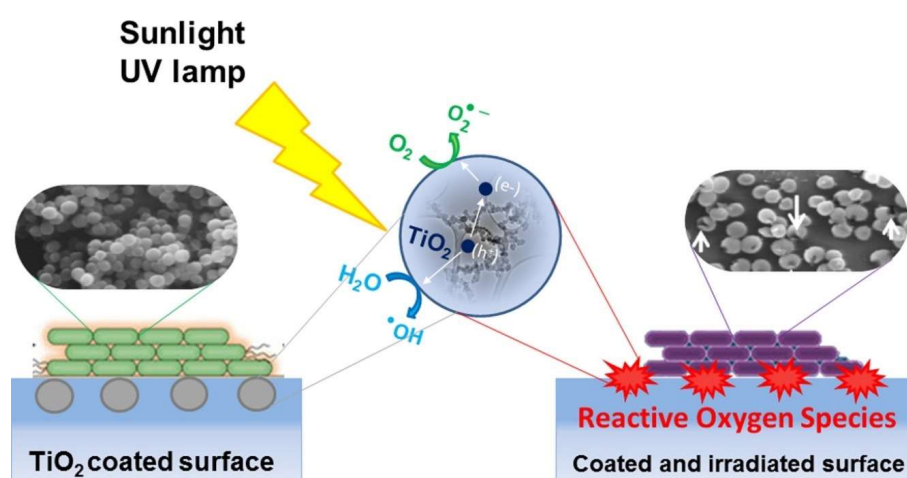# Antimicrobial and antibiofilm efficacy of self-cleaning surfaces functionalized by TiO$_2$ photocatalytic nanoparticles against *Staphylococcus aureus* and *Pseudomonas putida*

Antimicrobial and antibiofilm efficacy of self-cleaning surfaces functionalized by TiO$_2$ photocatalytic nanoparticles against *Staphylococcus aureus* and *Pseudomonas putida*

Blanca Jalvo[1], Marisol Faraldos[2,*], Ana Bahamonde[2], Roberto Rosal[1,*]

[1] Department of Chemical Engineering, University of Alcalá, E-28871 Alcalá de Henares, Madrid, Spain
[2] Instituto de Catálisis y Petroleoquímica, ICP-CSIC, Marie Curie 2, 28049 Madrid, Spain

* Corresponding authors: mfaraldos@icp.csic.es, roberto.rosal@uah.es

Abstract

A photocatalytic sol of TiO$_2$ nanoparticles has been used for creating self-cleaning antimicrobial flat and porous glass surfaces. The substrates were irradiated to study their photocatalytic properties and behavior in the presence of biofilm-forming bacteria. Smooth glass surfaces and glass microfiber filters were covered with $1.98 \cdot 10^{-3} \pm 1.5 \cdot 10^{-4}$ g·cm^{-2} and $8.55 \cdot 10^{-3} \pm 3.0 \cdot 10^{-4}$ g·cm^{-2} densities, respectively. Self-cleaning properties were analyzed using the methylene blue 365 nm UV-A photodegradation test. TiO$_2$-coated filters achieved rapid and complete photodegradation of methylene blue because of the better TiO$_2$ dispersion with respect to the glass slides. The effect of functionalized surfaces on the growth and viability of bacteria was studied using the strains *Staphylococcus aureus* and *Pseudomonas putida*. After irradiation (2 h, 11.2 W m^{-2}, 290–400 nm), the initially hydrophobic surface turned hydrophilic. The antibacterial effect led to extensive membrane damage and significant production of intracellular reactive oxygen species in all TiO$_2$-loaded irradiated specimens. The reduction of cell viability was over 99.9% (>3-log) for TiO$_2$ on glass surfaces. However, the polymeric extracellular matrix formed before the irradiation treatment was not removed. This study highlights the importance of bacterial colonization during dark periods and the difficulty of removing the structure of biofilms.

Keywords: photocatalysis; TiO$_2$; antimicrobial surface; bacterial biofilms; self-cleaning

1. Introduction

The development of self-cleaning surfaces constitutes an active research domain in materials science [1]. Self-cleaning can arise from manipulating surface wettability behavior and different chemical processes can be used to produce highly hydrophilic and superhydrophobic surfaces with antifogging or water repellence properties [2, 3]. An active research is being undertaken to find new superhydrophilic or superhydrophobic surfaces to create materials with application in many technological and biomedical fields [4]. Since the early discovery of its photoinduced superhydrophilicity, titanium dioxide has been used to prepare inorganic self-cleaning surfaces [5]. It has been suggested that UV irradiation resulted in the weakening of Ti-O lattice bonds leading to photogenerated surface hydroxyl groups in the presence of water [6]. Titanium dioxide has also been widely studied as heterogeneous photocatalyst based on its capacity to produce surface reactive oxygen species (ROS) such as the radicals HO$^{\bullet}$, O$_2^{\bullet-}$ or HO$_2^{\bullet}$ in a very well documented process [7]. Photocatalysis and photoinduced superhydrophilicity can take place simultaneously on the same surface, and their combination has widened the potential application of TiO$_2$ coatings as self-cleaning materials [8].

The photocatalytic properties of TiO$_2$ have also been used for creating antimicrobial surfaces. Photocatalytic disinfection has been proposed for creating antimicrobial building materials, medical devices and packaging films among a wide variety of materials and applications [7]. The photocatalytic water disinfection has been explored to overcome the risk of the disinfection by-products generated by the use conventional disinfectants [9]. Photocatalysis has proved capable of killing many microorganisms including bacterial endospores [10]. There is a clear evidence that the mode of action of photoactivated TiO$_2$ against bacteria is due to oxidative damage [11]. The oxidation of cell components can take place by direct contact with the catalyst surface or by the intermediation of ROS such as HO$_{\bullet}$ and H$_2$O$_2$ [12]. The production of O$_2^{\bullet-}$, the generation of bulk HO$^{\bullet}$ via Fenton mechanisms or the photodecomposition of H$_2$O$_2$ have also been proposed as sources of ROS in the process of bacterial inactivation [10]. As the photocatalytic reaction is surface contact dependent, the oxidative damage is much more important when cells and TiO$_2$ photoactivated surface are in close contact. This is the reason explaining the higher efficiency of nanoparticle suspensions in comparison with immobilized particles, which expose a much lower

surface area [13]. As expected, the kinetics of microorganism inactivation is highly dependent on the presence of radical scavengers [14].

A distinctive feature of biofilms from other colonizing infections is the presence of colonies of cells attached to a surface. Biofilm-mediated infections are responsible for the spreading of many diseases, particularly in the case of medical devices [15]. Bacterial colonization is also associated to foodborne diseases and leads to high economic losses in the food processing industry [16]. Biofilms are of particularly concern due to their resistance to host immune response mechanisms and to conventional disinfection processes [17]. The bacterial attachment and biofilm formation are complex processes that depend on several factors including the physicochemical properties of the surface, the temperature and pH, the availability of nutrients and the type of strain [18]. Once attached to a surface, bacteria form biofilms, which are structured aggregations of microorganisms consisting of cells immobilized and embedded within a polymeric matrix mainly made of exopolysaccharides. Significantly, bacteria in biofilms display unequaled metabolic versatility and phenotypic plasticity resulting in tolerance and resistance occurring within the biofilm environment [19, 20].

The efficacy of titanium dioxide photocatalyst for the inhibition of bacterial colonization has been widely explored, but the role played by biofilm matrix, and the removal of biofilms components has received much less attention. It has been shown that the photocatalytic activity of titanium dioxide considerably reduces bacterial populations in biofilms formed by the bacteria *Listeria monocytogenes* [21]. However, it has been reported that the efficiency of nanostructured TiO$_2$ coatings was lower for bacteria with high biofilm forming capacity [22]. The information available about impacts on bacterial biofilms as a whole is very limited. Xiao et al. found that the biofilm formation of *Escherichia coli* was substantially limited by UV/TiO$_2$, which was attributed to photogenerated active oxygen species interfering quorum sensing signals and the expression of biofilm-formation-related genes [23]. The impairment of biofilm communities by interfering the function of extracellular enzymes mediating the uptake of nutrients has also been reported [24]. However, the data available on the fate of the extracellular polymeric matrix in photocatalytic surfaces is very limited.

In this work, we prepared self-cleaning antimicrobial surfaces based on crystalline nanostructured TiO$_2$ exposed to simulated solar irradiation. The photooxidative damage produced to bacterial strains was studied using cultures of *Staphylococcus aureus* and *Pseudomonas putida*. The main goal of the article was to determine how surface characteristics influence the formation of biofilms on the TiO$_2$-functionalized material. The attention was focused on the antibacterial capacity against mature biofilms previously formed rather than on the inhibition of the initial colonization step, which is a topic extensively covered in the literature. Bacterial viability was tracked by using a combination of fluorescent dyes that allows differentiating viable and disrupted cells. The bacteria are considered non-viable when they suffered a damage in cell membranes. The intracellular formation of ROS was measured by means of a fluorescent probe. The visualization and quantification of biofilms was performed by staining the components of extracellular polymeric matrix. The results were cross-read to compare the antimicrobial and antibiofouling activities of the self-cleaning material.

2. Experimental

2.1. Preparation of photocatalytic materials

Suspensions of crystalline anatase TiO$_2$ nanoparticles were synthetized by sol-gel, typically adding 11.5 mL of titanium tetraisopropoxide (Sigma-Aldrich, 97%) to an acidic aqueous solution with a 140:1 water to nitric acid (Panreac, 65%) proportion, while stirring vigorously [25]. The suspension obtained was aged for three days and further dialyzed dialyzed using 3500 MWCO dialysis cassettes (ThermoFisher Scientific). The resultant suspension has a TiO$_2$ content of 20 ± 5 wt%. 2 mL of this TiO$_2$ 20 wt% preparation were extended over smooth glass slides 76×26 mm (VWR, Radnor, PA) and 47 mm, 1.6 μm pore size glass microfiber filters (Whatman International, Maidstone, UK). The TiO$_2$ suspension was spread by smearing in the case of the glass slides and by impregnation in the case of glass filters. Before and after the deposition, the coated substrates were dried at 110 °C and weighted to assess the amount of photocatalytic material deposited.

2.2. Characterization studies

The synthetized TiO$_2$ nanoparticle suspension was characterized for dynamic particle size by Dynamic Light Scattering (Malvern, Nanosizer), zero charge potential (Zeta-meter Inc. Model 3.0), surface acidity, shape and size of TiO$_2$ particles by TEM (JEOL 2100F) and TiO$_2$ loading by formation of the corresponding xerogel. BET specific surface area and micro-mesoporosity were obtained from nitrogen the adsorption-desorption isotherms of the TiO$_2$xerogel (Micromeritics, ASAP 2420) and from mercury porosimetry for the determination of meso-macropores and apparent density (Micromeritics, Poresizer 9520). Surface acidity was measured by ammonia chemisorption/physisorption isotherms (Micromeritics, ASAP 2010C). Band-gap was calculated from Tauc plots using UV–vis Diffuse Reflectance Spectroscopy (Agilent Cary 5000). Powder X-ray Diffraction (PANalytical X'Pert Pro) offered information about crystalline phases of TiO$_2$ and allowed estimating crystallite size by means of Scherrer's equation [26].

Titanium content was measured by plasma emission (ICP-OES, Perkin-Elmer Optima 330DV) of samples previously digested in acidic media into a microwave oven.

The wettability and hydrophilicity of coated and uncoated surfaces was tested using an optical contact angle meter (Krüss DSA25 Drop Shape Analysis System) using the sessile drop technique. Samples were placed on the test cell and drops of the testing liquids were placed on the surfaces by delivering syringe. The Surface free energy was determined by measuring contact angles (CA) with water (Milli-Q), glycerol, and diiodomethane. The components of the surface tension were estimated as described elsewhere [27, 28]. The procedure allowed calculating the free energy of interaction between two identical surfaces immersed in a liquid, ΔG_{SLS}, which gives a quantitative measurement of the hydrophobicity or hydrophilicity of the surface. If $\Delta G_{SLS} > 0$, the surface is hydrophilic, and if $\Delta G_{SLS} < 0$, it is hydrophobic. Details are included as Supplementary Material. Contact angle measurements for each surface were taken at room temperature on at least three different positions on each sample.

Scanning electron microscopy (SEM) images of the surface of materials were obtained using a Hitachi S-3000N microscope operating at 25 kV. The images of bacteria colonizing the surface of materials were taken in a ZEISS DSM-950 instrument. For this, a process of cell fixation in glutaraldehyde 5 % (v/v) in 0.2 M sodium cacodylate buffer pH 7.2 was carried out 1 h at room temperature. Samples were then rinsed in cacodylate buffer and dehydrated in an ascending ethanol series (25, 50, 70, 90 and 100%) before critical point drying with CO_2 and subsequent observation with SEM.

2.3. Photocatalytic activity studies

Two kinds of photodegradation test were used to assess the activity of TiO_2-functionalized surfaces. The anti-soiling chemical activity was studied using adsorbed organics under solid-solid conditions with methylene blue as probe compound. For the assessment of their effect on growth and viability of bacterial cells two biofilm-forming strains were used in a series of bioassays.

2.3.1. Self-cleaning activity: photocatalytic degradation of methylene blue

The degradation of adsorbed organics followed the procedure described elsewhere [29-31]. Dye photocatalytic degradation runs were performed in a closed and refrigerated camera (temperature was maintained at 25 ± 2 °C) equipped with six 15 W BBL fluorescent lamps, which emit in the UV-A range, centered at 365 nm. The samples were located at 20 cm of distance from lamps emitting 20 W m^{-2} irradiance in the 306–383 nm range, which was measured by a

broadband UV CUV-4 Kipp & Zonen radiometer. A spot of methylene blue (MB) was deposited on both substrates, slides and filters, by spraying with a nozzle regulated airbrush (Defynik 140 by Sagola) 5 mL of MB solution 5×10^{-4} M in acetone. Previously it was verified that the amount of MB provided enough color contrast. A calibration with five points was carried out to correlate measured reflectance and surface concentration of MB. For that purpose, 1 mL of MB 5×10^{-4} M solution was consecutively sprayed on certain areas of both supports after adjusting the distance to the surface of the airbrush nozzle. The dye photodegradation/bleaching was followed by taking micropictures (USB Microprobe Dino-Lite Edge AM4115ZT) and by measuring the diffuse reflectance spectra between 400–800 nm (where MB presents the maximum absorption) at different irradiation times in the 0–750 min interval. Parallel reference photodegradation runs were carried out with slides and filters without photocatalytic coating, and in the absence of irradiation.

2.3.2. Photo-bioassays and bioanalytical procedures

Irradiation experiments during bioassays were performed using a Heraeus TQ Xe 150 Xe-arc lamp with spectral emission mainly in the visible region with a minor contribution of UV-A (5.5% output in the 320–400 nm region, 94.2% > 400 nm). The lamp sleeve was equipped with a quartz cooling tube in which the lamps were fitted and was refrigerated by means of a thermostatic bath. The samples were irradiated at 15 cm from the lamp sleeve during 2 h after allowing 48 h for biofilm growth as indicated below. Fluence rate in the near UV was 11.2 W m^{-2} (measured in the 290–400 nm range), which was determined by chemical actinometry of 2-nitrobenzaldehyde [32]. The 290–400 nm range 5.8% of the total radian power emitted by the lamp.

Staphylococcus aureus (CECT 240) and *Pseudomonas putida* (CECT 4584) were used to test the antibacterial activity of TiO_2 photoactivated materials. The strains chosen are representative of biofilm-forming gram-positive and gram-negative bacteria respectively. *S. aureus* and *P. putida* were grown overnight in nutrient medium (beef extract 5 g/L, peptone 10 g/L, NaCl 5 g/L pH adjusted to 7.2), while shaking at 37 °C and 28 °C respectively. Exponentially growing cultures diluted to 10^8 cells/mL (optical density at 600 nm, OD$_{600}$ 0.0138, the same for both strains) were placed on the studied TiO_2 substrates and their corresponding control samples and incubated without stirring for 48 h in the dark at 37 °C, in the case of *S. aureus*, and at 28 °C in the case of *P. putida*. This procedure allowed the formation of mature but not irreversible biofilms on the photocatalytic surface, grown in pre-exposure dark period [33, 34]. The results proved that all cells resulted highly impaired after two hours of visible light irradiation, and that fouling due to accumulation of bacteria were not a barrier for the release of free

radicals from the photocatalytic surface. Surfaces continuously exposed to irradiation were not considered as they were permanently free of biofilms. Afterwards, the materials were carefully washed with distilled water to remove planktonic and loosely attached cells before the irradiation treatment. Biofilm formation assays were performed with and without TiO_2 on the surface of 96-well polystyrene plates following a modification of the method of Fletcher as a standard procedure [35]. For it, TiO_2 solution was deposited covering the surface of some wells to evaluate the biofilm formation ability of a surface completely covered with TiO_2. Polystyrene has been widely used as a reference plastic surface for cell adhesion and in this experiment, was considered as the control surface. After TiO_2 consolidation, bacterial incubation and irradiation treatment performed as described, the biofilm mass was quantified by measuring optical density. 200 μL of a crystal violet 0.1% solution were extended over the washed surface of each polystyrene well and incubated for 15 min to allow the staining of adhered cells. Excess stain was eliminated by rinsing with water. Plates were air dried and 1 mL of 95% ethanol was added to each well to extract crystal violet from cells. Distaining was performed overnight while gently shaking. Finally, the dye was measured at OD_{590}. Every measurement was performed twelve times for each experimental condition. For the visualization of the extracellular polymeric matrix, the biofilms were stained with 200 μL FilmTracer SYPRO Ruby (Molecular Probes, Invitrogen) per sample, incubated in the dark for 30 min at room temperature, and rinsed with distilled water. Then, they were observed using confocal microscopy (Confocal SP5, Leica Microsystems, Germany) with excitation/emission wavelengths of 450 nm and 610 nm respectively.

Bacterial viability assays were performed using LIVE/DEAD BacLight Bacterial Viability Kit (Molecular Probes, Invitrogen Detection Technologies, Carlsbad, CA, USA). Under LIVE/DEAD staining, all cells exhibit green fluorescence (SYTO 9), whereas nonviable bacterial cells display red fluorescence

(Propidium iodide, PI) with dye uptake depending upon cell membrane integrity. For the staining of films 10 μL of BacLight stain (a mixture of SYTO 9 and PI in DMSO, following the manufacturer's recommendations) were used. The incubation was performed in the dark for 15–30 min at room temperature. For green fluorescence (SYTO 9) excitation was performed at 488 nm and emission at 500–575 nm. For red fluorescence (PI, dead cells), the excitation/emission wavelengths were 561 nm and 570–620 nm respectively.

The oxidative stress suffered by bacterial cells on coated and uncoated surfaces was measured after 48 h of biofilm formation using 2′,7′-dichlorodihydrofluorescein diacetate (H_2DCFDA). 50 μL of a 10 mM H_2DCFDA stock solution were added to each sample and incubated for 1 h at room temperature. This probe is cell-permeable and undergoes intracellular hydrolysis to yield the dichlorodihydrofluorescein (DCFH) carboxylate anion, which is retained in the cell. Two-electron oxidation of DCFH results in the formation of dichlorofluorescein (DCF), which is fluorescent compound that serves as an indicator for hydrogen peroxide and other ROS, such as hydroxyl and peroxyl radicals [36]. The intracellular generation of DCF was monitored by confocal fluorescence microscopy with excitation at 488 nm and emission at 655 nm.

2.4. Statistical analysis

Means and standard deviation values were calculated from experiments replicated until obtaining reliable results. Statistical analyses were performed by using R software 3.0.2. (The R Foundation for Statistical Computing©). Statistically significant differences were considered to exist when $p < 0.05$.

3. Results and Discussion

The main physicochemical properties of TiO_2 nanoparticles suspension and the TiO_2xerogel, prepared by solvent evaporation at room temperature, are presented in Table 1. The synthetized suspension

Table 1. Physicochemical properties of TiO_2 suspension and xerogel.

| TiO₂ suspension		Coated TiO₂ xerogel	
TiO_2 (wt%)	20 ± 2	Ti content (wt%)	54 ± 5
pH	3.0 ± 0.5	Band-gap (eV)	3.14 ± 0.06
Isoelectric point	5.1 ± 0.5	Crystalline phase	TiO_2 anatase
ζ-potential (pH 7.0, mV)	34.0 ± 0.5	$d_{crystallite}$ (nm)	3.8 ± 0.2
DLS particle size (nm)	$4 \pm 1, 16 \pm 3, 65 \pm 6$	S_{BET} (m²/g)	340 ± 15
Primary particle size (TEM, 500 particles, nm)	5.6 ± 1.4	V_{pore} (cm³/g)	0.22 ± 0.08
		d_{pore} (nm)	3.4 ± 0.5
		Density (g/cm³)	2.7831 ± 0.008
		Acidity (meq H^+/g)	1.28 ± 0.04

presents 20% anatase-TiO$_2$ content and is stabilized after dialyzation at pH 3.0. The primary particle size is around 4–5 nm as verified by TEM. The details are given in Fig. 1. DLS also showed the presence of secondary particles due to aggregation. The high surface area, porosity and acidity found in the formed xerogel confirmed the noteworthy physicochemical properties of the prepared nanostructured TiO$_2$ suspension to perform photocatalytic coatings. The X-ray diffractogram in in Fig. 1 proved the only presence of anatase crystalline phase.
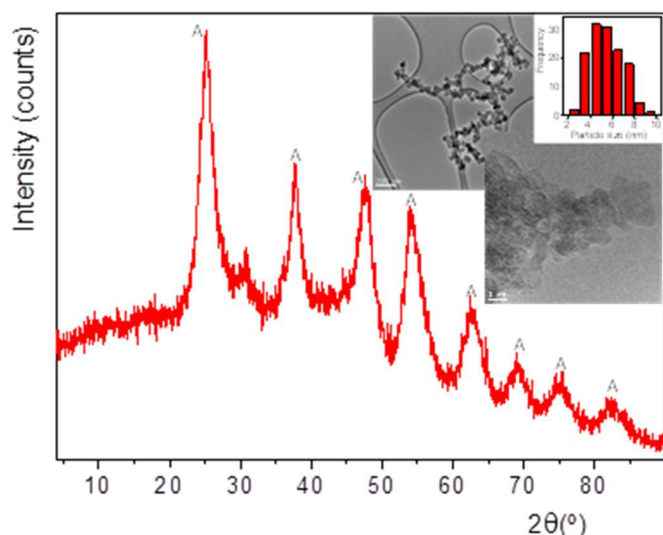
Figure 1. X-ray diffractogram, TEM images and particle size histogram of prepared TiO2 xerogel.

size of particles corresponded to that of the TiO$_2$ material as noted before (close-up of Fig. 2B). The material dispersed in glass filters displayed similar aggregates, spread in smaller plates adhered to filter fibers or occupying the pores defined by them (Fig. 2C). Overall, the total amount of TiO$_2$ per unit surface was considerably lower when deposited in filters, but the dispersion was better due to the role of glass fibers in creating a pattern of microsized sheets.
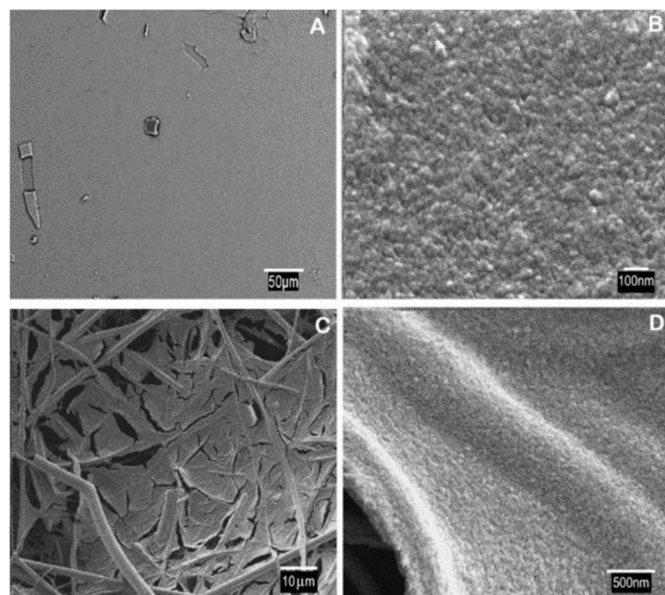
Figure 2. SEM images of TiO2-coated glass slides (A and B), TiO2-coated filters (C and D).

The surface density of TiO$_2$ on glass microfiber filters was $1.98 \cdot 10^{-3} \pm 1.5 \cdot 10^{-4}$ g cm^{-2}, whereas the coverage layer deposited on glass slides amounted to $8.55 \cdot 10^{-3} \pm 3.0 \cdot 10^{-4}$ g cm^{-2}. The values for the glass slides were calculated considering the surface on which the TiO$_2$ gel was smeared, which was 55×26 cm, excluding the frosted end of the slide. Fig. 2 (A and B) shows typical SEM micrographs of the TiO$_2$ material on glass slides and filters. When deposited on glass slides, TiO$_2$ forms homogeneous layers of tight aggregates of particles displaying planar surfaces with some irregularities as shown in Fig. 2A. The primary

Table 2 gives the values of surface energy components for bare, irradiated and non-irradiated glass slides as well as for bacterial lawns. The value for the total solid-liquid interfacial energy, γSLW, was 38.6 mJ m^{-2} for TiO$_2$ deposited on glass slides, which dropped to 23.2 mJ m^{-2} upon Xe-arc light irradiation. The figures were similar to the values reported elsewhere for comparable materials [37]. The surface of TiO$_2$/slides was hydrophobic, with considerably negative ΔG_{SLS} values. Upon irradiation, the surface turned hydrophilic with $\Delta G_{SLS} = +70 \pm 9$ mJ m^{-2}. It is a well-known fact that TiO$_2$ surfaces exhibit a photo-induced

Table 2. Surface characterization by means of contact angle measurements and derived surface energy components (mJ/m^2).

Material	θ_{water}	$\theta_{glycerol}$	$\theta_{diiodomethane}$	γ_S^{LW}	γ_S^+	γ_S^-	γ_S^{AB}	γ_S	ΔG_{SLS}
Glass slides	39.7 ± 3.5	42.5 ± 0.7	60.7 ± 0.4	28.2	0.02	5.90	0.75	28.9	-52 ± 8
TiO$_2$/slides	57.9 ± 3.9	71.9 ± 4.8	42.0 ± 2.6	38.6	0.02	0.05	0.06	38.6	-100 ± 11
TiO$_2$/slides*	34.3 ± 1.7	6.5 ± 2.4	1.3 ± 0.5	22.7	-	73.1	0.54	23.2	+70 ± 9
S. aureus	21.8 ± 4.6	76.4 ± 5.5	88.2 ± 5.3	13.6	0.01	106	1.69	15.3	+102 ± 15
P. putida	15.6 ± 2.8	63.2 ± 3.5	58.9 ± 3.7	29.2	1.44	62.3	18.9	48.2	+42 ± 8

* irradiated for 5 min, 25 °C

wettability transition, which leads to a decreased water contact angle following irradiation. This phenomenon has been attributed to the breaking of Ti-O lattice bonds by photogenerated holes. Water molecules would then coordinate the titanium site leading to an increase in the number of surface hydroxyl groups. As the newly formed hydroxyl groups are less stable than the initial doubly coordinated hydroxyl groups, the material restores its initial hydrophobicity in the space of a few hours after irradiation [38].

3.1. Self-cleaning photocatalytic activity

The efficiency of the photooxidative process upon irradiation of slides and filters in contact with MB is shown in form of a full series of micropictures in Fig. S1 of Supplementary Material. Reference filters and slides without coating were used as blank (B) to discard MB photochemical degradation. As observed in Fig. S1 the stain color was practically maintained along the 750 min irradiation period for blanks, while significant discoloration appeared in coated slides (slides 1 and 2) that exhibited only a residual heterogeneous speckled surface after irradiation. The samples of TiO2-coated filters achieved complete photodegradation with negligible MB stain beyond 300 minutes. The photodegradation of MB, quantified by diffuse reflectance spectroscopy, is shown in Fig. 3 for filters

(A) and slides (B). Blanks are also shown to verify the absence of MB photochemical degradation. The photocatalytic process progresses rapidly during the first 300 min, to slow down at longer irradiation times. The behavior on both supports was reproducible as observed with replicates.

MB photodegradation rate was one order of magnitude higher for filters than for slides, both in terms of photoreaction rate and semi-reaction time. Table 3 shows the calculated values for MB photo-oxidation rate expressed per unit surface and per unit mass of TiO_2. MB photo-oxidation efficiency was particularly high in the case of TiO_2 coating on glass filters with values around 50-fold higher than that of glass slides when expressed per unit mass of TiO_2, that could be well explained as a consequence of the best dispersion of TiO_2 coating on glass filters. As noted before, TiO_2 material deposited on glass slides formed a homogeneous layer where the photoactive surface was flat following the shape of the covered support. Accordingly, half MB photodegradation time was one order of magnitude lower for TiO_2 coated filters, even when the amount of TiO_2 deposited on them was four times lower, revealing noteworthy self-cleaning performance.
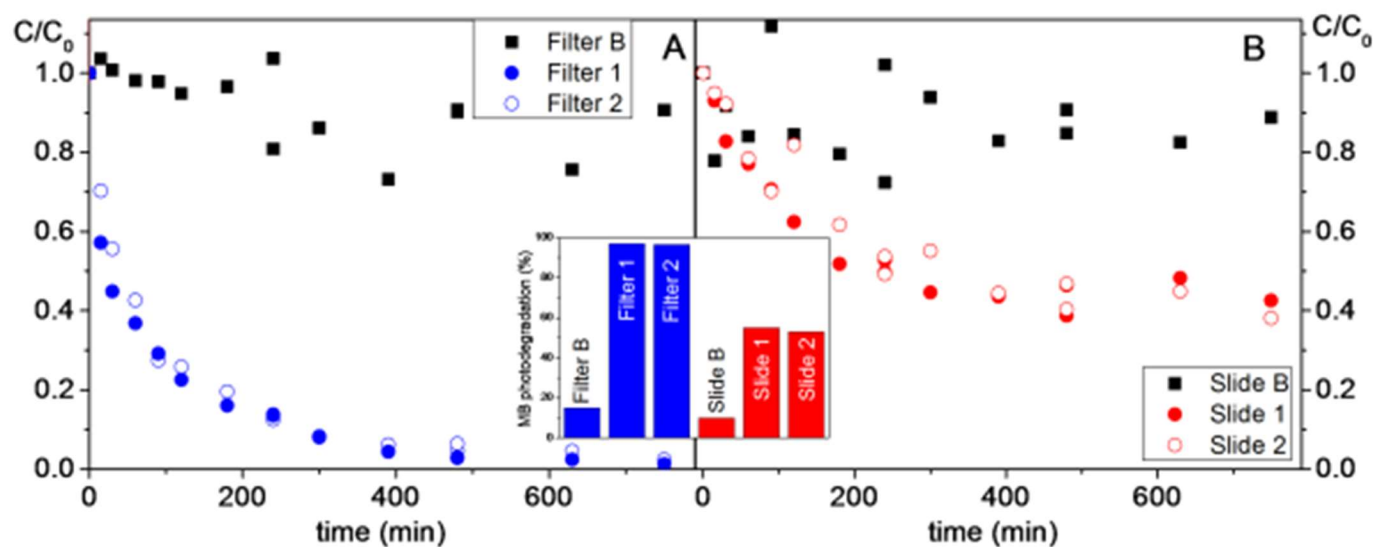
Figure 3. Evolution of MB concentration with irradiation time for TiO2-coated filters (A) and TiO2-coated slides (B). MB photodegradation at 400 min (inset).

Table 3. Values of r_o and $t_{1/2}$ during MB photocatalytic degradation on slides and filters.

Kinetic Parameters	Slides		Filters	
	Blank	TiO2-coated	Blank	TiO2-coated
$t_{1/2}$ (min)	-	232 ± 11	-	27 ± 10
r_o (mmol·cm^{-2}·min^{-1})	0.013 ± 0.009	0.078 ± 0.004	0.025 ± 0.009	0.97 ± 0.23
r_o (µmol·g^{-1}·min^{-1})	-	0.0091 ± 0.0005	-	0.49 ± 0.11

3.2. Antimicrobial performance

The effect on bacterial viability was studied using LIVE/DEAD staining and confocal microscopy. The confocal micrographs shown in Fig. 4 correspond to slides and filters with, C(+), and without, C(−), TiO$_2$ coating and in irradiated, L(+), and non-irradiated, L(−) samples. The growth of both strains, *P. putida* and *S. aureus*, was clear in control materials on which a considerable amount of viable green-labelled cells were visible. Xe-lamp irradiation did not induce bacterial damage in the absence of TiO$_2$, but cell impairment was apparent for TiO$_2$-irradiated materials. The cells on TiO$_2$-functionalized slides and filters showed extensive cell photo-impairment, with practically all cells red-marked. Red-marked cells were those internalizing PI and, therefore, suffering damage in cell membrane integrity. Certain cells appeared yellowish or orange. Yellow cells are generally considered viable, while orange cells can be considered damaged [39]. A certain amount of bacteria appeared yellow-to-orange in C(+) L(−) samples (samples with TiO$_2$ but kept in the dark). The effect may be associated to the irradiation suffered during confocal microscopy observations. Cell counting using the public domain Java image processing software ImageJ on at least three independent fields allowed estimating the reduction in cell viability upon irradiation, which amounted to >3-log for C(+) L(+) samples except for *P. putida* on glass filters, for which the number of yellow/green-marked
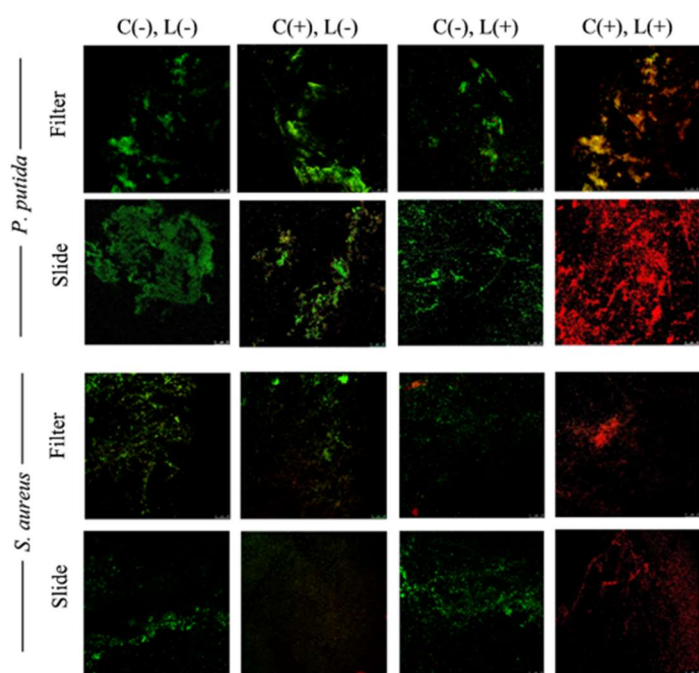
Figure 4. Live/Dead confocal micrographs of *P. putida* and *S. aureus* on TiO$_2$-coated glass filters and TiO$_2$-coated glass slides in irradiated, L(+), and no-irradiated, L(−), samples. Irradiation Conditions: 2 h under Xe arc lamp after 48 h in the dark at 28 °C (*P. putida*) or 37 °C (*S. aureus*). C(+): samples with TiO$_2$, C(−): control samples.

viable cells was roughly 10% of the total. The difference was attributed to the higher surface available for bacterial attachment and to the existence of shadowed shelters in them.

The cause for damage in bacterial cells exposed to photocatalytic irradiated material was the production of ROS as intermediates of oxygen-dependent photosensitized reactions. This was measured as DCF fluorescence intensity and recorded as confocal micrographs in Fig. 5. The images on top are micrographs showing *P. putida* and *S. aureus* cultures kept for 48 h on TiO$_2$-functionalized slides and filters and subsequently irradiated for 2 h using Xe-arc lamp. All TiO$_2$-functionalized materials showed intense intracellular green DCF fluorescence because of ROS production. The confocal images on top correspond to filters and slides with TiO$_2$ but non-irradiated (A, E, C and G), and irradiated TiO$_2$-loaded filters (B and F) and slides (D and H). The quantification of ROS production was performed by digitally converting the images into pixels. Every image was treated to enhance contrast and pixels were transformed into percent surface using ImageJ. The results are also shown in Fig. 5 for *P. putida* (I) and *S. aureus* (J). Non-TiO$_2$ loaded specimens, C(−), and those kept in the dark, L(−), exhibited non-significant differences in DCF fluorescence intensity. Conversely, for TiO$_2$-functionalized and irradiated filters and slides, the increase in the intensity of the DCF signal was substantial, and higher in slides than in filters probably due to the greater load of photocatalytic material of the former.

The antimicrobial effect of TiO$_2$ materials has been linked before to membrane integrity destabilization and oxidative toxicity due to the generation of hydroxyl radicals and other species that affects bacterial activity and growth rates [40, 41]. Fig. 6 and Fig. S2 (Fig. 6 proofs cell damage while Fig. S2, with lower magnification, allows biofilm visualization) show SEM micrographs that detail the morphology changes of *P. putida* and *S. aureus* cells upon irradiation treatments in contact with TiO$_2$ nanomaterial. In non-irradiated samples, the morphology (rod shaped) of *P. putida* cells was retained (Fig. 6A and E). However, after 2 h irradiation, the surface of *P. putida* cells appeared wrinkled and irregular with some cells clearly evidencing damaged membranes (arrows in Fig. 6B and 6F). Also, for *S. aureus* cell irradiated on TiO$_2$-functionalizaed surface presented important morphology alterations, in contrast with the smooth cell contours of normal bacteria. Fig. 6D and H show collapsed and lysed cells compared to normal cells in Fig. 6C and G. It is a well-known fact that membrane integrity disruption leads to a reduced ability to control the movement of substances in and out of a bacterial cell, eventually causing cell death. The morphological
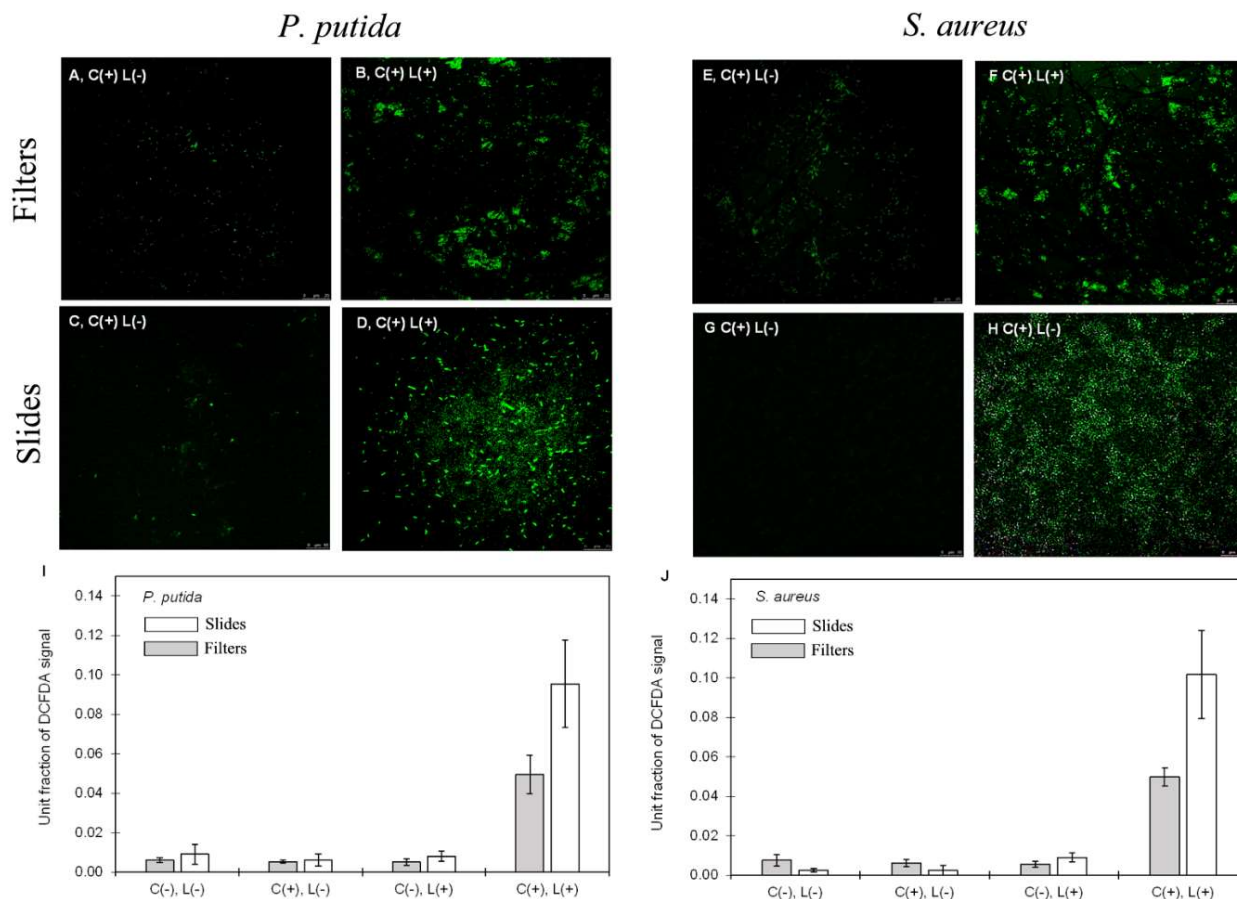
Figure 5. Confocal microscopy images of *P. putida* (A, B, C, D) and *S. aureus* (E, F, G, H) bacterial cultures on TiO_2 materials showing intracellular green DCF fluorescence because of ROS production. A, B, E and F: filters; C, D, G and H: slides. Figures I and J: grey bars: filters; white bars: slides. C(+): samples with TiO_2, C(-): controls, L(+): irradiated, L(-): non-irradiated. Irradiation conditions: 2 h under Xe arc lamp after 48 h in the dark
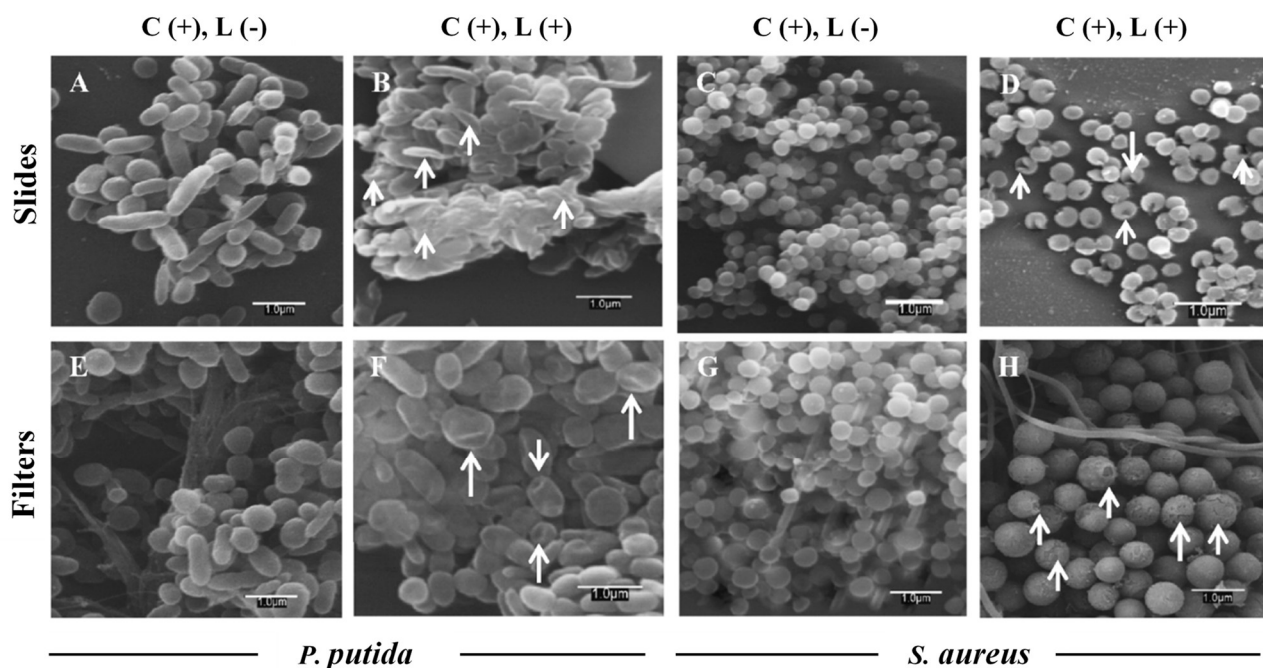

Figure 6. SEM images of *P. putida* (A, B, E and F) and *S. aureus* (C, D, G and H) biofilms on TiO_2-coated glass slides (A, B, C and D) and TiO_2-coated filters (E, F, G and H) before (A, C, E and G) and after irradiation (B, D, F and H).

alterations observed agree with the rest of results presented before on the antibacterial effect of TiO$_2$ nanomaterial.

Bacterial colonization not only refers to the attachment of free bacteria to a given surface, but mainly to the formation of structured aggregations of microorganisms and the extracellular polymeric matrix jointly referred to as biofilm. The extracellular polymeric substances (EPS) of microbial biofilms provide the structural stability as well as protection to the biofilm cells and, in fact, one of the main roles of extracellular proteins is to facilitate the initial colonization steps by planktonic cells. EPS is also composed by enzymes, which enable the digestion of exogenous macromolecules for nutrient acquisition and the degradation of structural biofilm macromolecules to release free cells for new colonization processes, among other functions [42]. Biofilm formation visualized using the FilmTracer SYPRO Ruby biofilm matrix stain, which labels most classes of EPS proteins, is shown in Fig. 7. The results showed that biofilm formation took place in all samples. It was also observed (Fig. S3 Supplementary material) that non-irradiated TiO$_2$-coated surfaces displayed higher amount of EPS for both strains than control filters and slides. The irradiation, either in the presence or absence of TiO$_2$ coatings did not modify the amount of biofilm as revealed by the stain.
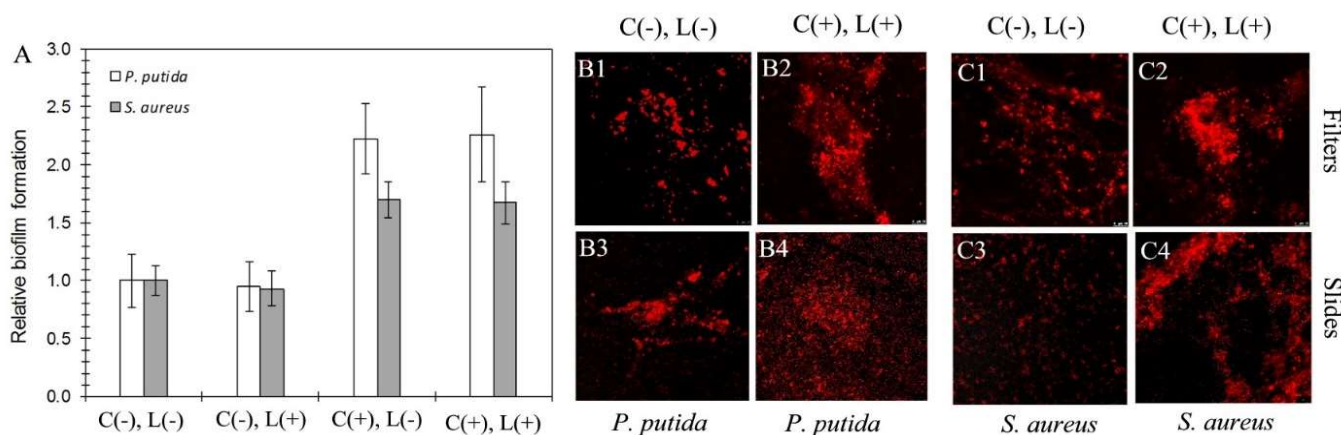
Figure 7. Left side (A): quantification of biofilms on polystyrene wells by means of the crystal violet method (A). C(-): control wells, C(+): wells with TiO$_2$, L(-): non-irradiated, L(+): irradiated. Right-side panel: FilmTracer SYPRO Ruby biofilm matrix staining of filters and slides comparing control samples (B1, B3, C1 and C3) and TiO$_2$-coated and irradiated filters (B2, C2) and slides (B4, C4).

The quantification of biofilm formation was also performed by crystal violet staining on TiO$_2$ deposited on the bottom surface or polystyrene plates as described before. The experiment was designed to quantify the effect of TiO$_2$ and its Xe-arc light irradiation with the conventional method used to quantify biofilm density in bacterial cultures [43]. The results are shown in Fig. 7A in which the bars correspond to relative biofilm formation (1 for non-irradiated control) together with their 95% confidence intervals. The amount of biofilm formed was higher for samples with TiO$_2$, which roughly doubled the amount measured by crystal violet staining with respect to controls without TiO$_2$ in agreement with the results provided by FilmTracer SYPRO Ruby micrographs. In fact, both methods offer complementary information on biofilm components. While crystal violet nonspecifically stains all cells attached to the surface, viable or not, and the EPS matrix, FilmTracer SYPRO Ruby preferentially binds proteins, which are the components providing structural stability to biofilms. Therefore, both using crystal violet and SYPRO Ruby staining it was demonstrated that the irradiation of TiO$_2$-functionalized slides or filters, did not suppose a reduction in the amount of biofilm and that TiO$_2$-coated surfaces were more easily colonized than the corresponding filters, slides or polystyrene pristine materials.

TiO$_2$-functionalized surfaces were more susceptible to bacterial colonization, which can be explained by the different surface topography, which offered more adhesion points for bacterial anchoring structures. Another possible explanation is the a more favorable energy of interaction. Table 2 displays the calculated values of ΔG_{SLS} for glass slides with and without TiO$_2$ and the latter after 5 min visible light irradiation and lawns of the two bacterial strains used in this work. The free energy of interaction, ΔG_{SLS}, gives a measure of the hydrophobicity or hydrophilicity of the surface. When $\Delta G_{SLS} > 0$, the surface is hydrophilic, and when $\Delta G_{SLS} < 0$, it is hydrophobic. No values were recorded for glass filters because probe liquids rapidly spread on their surface making it impossible to measure contact angles. Glass slides were initially hydrophobic and turned even more hydrophobic when covered with TiO$_2$, reaching $\Delta G_{SLS} = -100$ mJ m^{-2}. Irradiation, however, renders TiO$_2$ films hydrophilic, with particularly high electron donor component, γ_S^-, of the

surface energy. This is consistent with the data showing that the increase of the hydrophilicity of irradiated TiO_2 can be attributed to the increase of the surface hydroxyl groups formed from photogenerated surface holes [6]. The data shown in Table 2 indicated that both strains were highly hydrophilic, with ΔG_{SLS} values positive and close to those of irradiated TiO_2-covered slides.

The maximum interaction expected between two surfaces takes place if the difference in hydrophilicity is not high. However, bio-surface interactions are more complex. First, hydrophobic and steric interactions have been found to play a significant role in bacterial adhesion [44]. Second, the pure thermodynamic approach assumes direct contact between bacteria and surface, which is not true in the presence of cell appendages, such as pili and flagella as well as the EPS segregated by biofilm forming microorganisms [45]. Third, culture media contain many adsorbable organic and inorganic compounds, which complicate the use of physicochemical models [46]. Additionally, photo-responsive surfaces can be modified by the irradiation potentially leading to drastic changes in the ability of microorganisms to colonize them [47]. It has also been pointed out that there is a strong relationship between bacterial adhesion and surface roughness [48]. Smooth surfaces do not favor bacterial adhesion, which may explain why the more hydrophobic TiO_2-covered glass slides displayed more biofilm formation.

The reduction of biofilm forming bacteria on photocatalytic surfaces has been described elsewhere. Wolfrum et al., studied the photocatalytic oxidation of bacteria, spores, and biofilms by measuring carbon dioxide evolution during the irradiation of quartz disks treated with TiO_2 nanoparticles (P25) and found high mineralization degrees in less than 24 h upon UV (365 nm) irradiation at a fluence rate of 104 W m^{-2} [49]. In another work, *Streptococcus mutans* was cultured on a TiO_2 photocatalytic surface for 16 h before irradiation with UV-A (371 nm) resulting in 5–6 orders of magnitude reduction in the number of viable bacteria for a dose of 43 J cm^{-2} (1 h, irradiance 120 W m^{-2}) [50]. For comparison, the near-UV (290–400 nm) solar irradiance monthly average at earth's surface is in the 2.0-13.8 W m^{-2} range [51], which is one order of magnitude lower and similar to the value used in this work. Our work showed that almost complete cell impairment of colonizing bacteria could be attained using the TiO_2 nanomaterial described here at realistic UV exposures. The MB removal activity per unit mass of TiO_2 was higher in filters, but ROS-induced cell damage was higher in the case of slides. This result can be rationalized in terms of the surface structure of both materials because the flat surface of slides offers fewer possibilities for bacterial colonization and less shadowed shelters. In fact, as shown in several images of Fig. S2 and S3, bacteria tend to grow close to the glass fibers in filters, the lower part of which was relatively protected from the oxidative photo-impairment. Another interesting interaction between photocatalytic surfaces and microorganisms is encountered in the electrochemically active biofilms produced by a variety of naturally occurring microorganisms [52]. The electrochemical interaction between biofilms and titanium dioxide nanoparticles has been used to create several types of composite nanoparticles using the electrons produced by the oxidation of substrates by the microorganisms in the biofilm, which are injected into the conduction band of photocatalytic nanoparticles [53].

In this work, biofilm formation took place during the contact with microbial cultures prior to irradiation. The results showed that even if bacterial cells could be completely impaired by ROS, the extracellular polymeric matrix could not be removed on TiO_2-functionalized surfaces once the formation of a biofilm took place. Some studies concluded that the resistance of bacterial populations towards antibacterial engineered nanomaterials depends on the initial cell density, dense cultures being more resistant than the less ones [54]. In our study, despite the high density of bacterial populations used, most of the biofilm cells were damaged and render non-viable due to the photocatalytic effect of TiO_2. However, the irradiation had no effect on the amount of biofilm remaining after the exposure-treatment cycle proving that the biofilm architecture was not destroyed. Our results showed that the photocatalytic activity leading to complete cell impairment was unable to remove the extracellular structure of a mature biofilm, a result that has not been previously reported for self-cleaning surfaces and is important for practical applications, naturally subjected to light-darkness cycles.

4. Conclusions

TiO_2 nanoparticles consisting of anatase with a primary particle size of about 5 nm were used to functionalize glass microfiber filters and glass slides with a density of $1.98 \times 10^{-3} \pm 1.5 \times 10^{-4}$ g cm^{-2} and $8.55 \times 10^{-3} \pm 3.0 \times 10^{-4}$ g cm^{-2} respectively. TiO_2-functionalizaed surfaces were hydrophobic and turned hydrophilic upon simulated solar irradiation. The photocatalytic activity was assessed using the MB photodegradation test upon UV-A irradiation at 365 nm. TiO_2-coated filters achieved total MB photo-oxidation with a photodegradation rate 50 times higher than coated slides, which was attributed to the higher photoactive surface of glass fiber filters.

The biofilm-forming bacteria *Staphylococcus aureus* and *Pseudomonas putida* grew easily on TiO_2-functionalized filters and glass slides. After 2 h of visible/near UV light (11.2 W m^{-2} in the 290–400 nm range) irradiation practically all cells became non-

viable evidencing clear membrane damage. Significant production of ROS was detected using an intracellular stain in all TiO$_2$ irradiated specimens. The biofilm tracking assays performed in this work showed that the photooxidation induced by TiO$_2$, although impairing essentially all bacterial cells, but was unable to remove the biofilm matrix formed during a period of darkness prior to irradiation.

Acknowledgements

References

[1] K. Liu, L. Jiang, Bio-inspired self-cleaning surfaces, Annual Review of Materials Research, 42 (2012) 231-263.

[2] K.T. Huang, S.B. Yeh, C.J. Huang, Surface modification for superhydrophilicity and underwater superoleophobicity: Applications in antifog, underwater self-cleaning, and oil–water separation, ACS Appl. Mater. Interfaces, 7 (2015) 21021-21029.

[3] S. Nishimoto, B. Bhushan, Bioinspired self-cleaning surfaces with superhydrophobicity, superoleophobicity, and superhydrophilicity, RSC Advances, 3 (2013) 671-690.

[4] B. Su, Y. Tian, L. Jiang, Bioinspired interfaces with superwettability: From materials to chemistry, J. Am. Chem. Soc., 138 (2016) 1727-1748.

[5] R. Wang, K. Hashimoto, A. Fujishima, M. Chikuni, E. Kojima, A. Kitamura, M. Shimohigoshi, T. Watanabe, Light-induced amphiphilic surfaces, Nature, 388 (1997) 431-432.

[6] N. Sakai, A. Fujishima, T. Watanabe, K. Hashimoto, Quantitative evaluation of the photoinduced hydrophilic conversion properties of TiO$_2$ thin film surfaces by the reciprocal of contact angle, The Journal of Physical Chemistry B, 107 (2003) 1028-1035.

[7] K. Nakata, A. Fujishima, TiO$_2$ photocatalysis: Design and applications, Journal of Photochemistry and Photobiology C: Photochemistry Reviews, 13 (2012) 169-189.

[8] C. Euvananont, C. Junin, K. Inpor, P. Limthongkul, C. Thanachayanont, TiO$_2$ optical coating layers for self-cleaning applications, Ceramics International, 34 (2008) 1067-1071.

[9] O.K. Dalrymple, E. Stefanakos, M.A. Trotz, D.Y. Goswami, A review of the mechanisms and modeling of photocatalytic disinfection, Applied Catalysis B: Environmental, 98 (2010) 27-38.

[10] H.A. Foster, I.B. Ditta, S. Varghese, A. Steele, Photocatalytic disinfection using titanium dioxide: spectrum and mechanism of antimicrobial activity, Appl. Microbiol. Biotechnol., 90 (2011) 1847-1868.

[11] Y. Cai, M. Strømme, K. Welch, Disinfection kinetics and contribution of reactive oxygen species when eliminating bacteria with TiO$_2$ induced photocatalysis, Journal of Biomaterials and Nanobiotechnology, 5 (2014) 200.

[12] T. Sato, M. Taya, Copper-aided photosterilization of microbial cells on TiO$_2$ film under irradiation from a white light fluorescent lamp, Biochemical Engineering Journal, 30 (2006) 199-204.

[13] V. Cohen-Yaniv, N. Narkis, R. Armon, Photocatalytic inactivation of *Flavobacterium* and *E. coli* in water by a continuous stirred tank reactor (CSTR) fed with suspended/immobilised TiO$_2$ medium, Water Sci. Technol., 58 (2008) 247-252.

[14] M. Cho, H. Chung, W. Choi, J. Yoon, Linear correlation between inactivation of *E. coli* and OH radical concentration in TiO$_2$ photocatalytic disinfection, Water Res., 38 (2004) 1069-1077.

[15] L. Hall-Stoodley, J.W. Costerton, P. Stoodley, Bacterial biofilms: from the natural environment to infectious diseases, Nature Reviews Microbiology, 2 (2004) 95-108.

[16] H.P. Blaschek, H.H. Wang, M.E. Agle, Biofilms in the Food Environment, 2007.

[17] C. de la Fuente-Núñez, F. Reffuveille, L. Fernández, R.E.W. Hancock, Bacterial biofilm development as a multicellular adaptation: antibiotic resistance and new therapeutic strategies, Current Opinion in Microbiology, 16 (2013) 580-589.

[18] R. Van Houdt, C.W. Michiels, Biofilm formation and the food industry, a focus on the bacterial outer surface, Journal of Applied Microbiology, 109 (2010) 1117-1131.

[19] P. Gilbert, J. Das, I. Foley, Biofilm Susceptibility to Antimicrobials, Advances in Dental Research, 11 (1997) 160-167.

[20] M.E. Shirtliff, J.T. Mader, A.K. Camper, Molecular interactions in biofilms, Chemistry and Biology, 9 (2002) 859-871.

[21] N.G. Chorianopoulos, D.S. Tsoukleris, E.Z. Panagou, P. Falaras, G.J.E. Nychas, Use of titanium dioxide (TiO$_2$) photocatalysts as alternative means for *Listeria monocytogenes* biofilm disinfection in food processing, Food Microbiology, 28 (2011) 164-170.

[22] B. Jeffery, M. Peppler, R.S. Lima, A. McDonald, Bactericidal effects of HVOF-sprayed nanostructured TiO$_2$ on *Pseudomonas aeruginosa*, Journal of Thermal Spray Technology, 19 (2010) 344-349.

[23] X. Xiao, W.W. Zhu, Q.Y. Liu, H. Yuan, W.W. Li, L.J. Wu, Q. Li, H.Q. Yu, Impairment of biofilm formation by TiO$_2$ photocatalysis through quorum quenching, Environ. Sci. Technol., 50 (2016) 11895-11902.

[24] H. Schug, C.W. Isaacson, L. Sigg, A.A. Ammann, K. Schirmer, Effect of TiO$_2$ nanoparticles and UV radiation on extracellular enzyme activity of intact heterotrophic biofilms, Environ. Sci. Technol., 48 (2014) 11620-11628.

[25] D.H. Kim, M.A. Anderson, W.A. Zeltner, Effects of firing temperature on photocatalytic and photoelectrocatalytic properties of TiO$_2$, Journal of Environmental Engineering, 121 (1995) 590-594.

[26] R. Jenkins, R.L. Snyder, Index, in: Introduction to X-ray Powder Diffractometry, John Wiley & Sons, Inc., 1996, pp. 397-403.

[27] C.J. van Oss, Development and applications of the interfacial tension between water and organic or biological surfaces, Colloids and surfaces B: Biointerfaces, 54 (2007) 2-9.

[28] C.J. Van Oss, M.K. Chaudhury, R.J. Good, Interfacial Lifshitz-van der Waals and polar interactions in macroscopic systems, Chem. Rev., 88 (1988) 927-941.

[29] A. Ojstršek, K.S. Kleinschek, D. Fakin, Characterization of nano-sized TiO_2 suspensions for functional modification of polyester fabric, Surface and Coatings Technology, 226 (2013) 68-74.

[30] I. Alfieri, A. Lorenzi, L. Ranzenigo, L. Lazzarini, G. Predieri, P.P. Lottici, Synthesis and characterization of photocatalytic hydrophobic hybrid TiO_2-SiO_2 coatings for building applications, Building and Environment, 111 (2017) 72-79.

[31] J. Zhou, Z. Tan, Z. Liu, M. Jing, W. Liu, W. Fu, Preparation of transparent fluorocarbon/TiO_2-SiO_2 composite coating with improved self-cleaning performance and anti-aging property, Appl. Surf. Sci., 396 (2017) 161-168.

[32] J.M. Allen, S.K. Allen, S.W. Baertschi, 2-Nitrobenzaldehyde: A convenient UV-A and UV-B chemical actinometer for drug photostability testing, Journal of Pharmaceutical and Biomedical Analysis, 24 (2000) 167-178.

[33] S.P. Diggle, K. Winzer, S.R. Chhabra, K.E. Worrall, M. Cámara, P. Williams, The *Pseudomonas aeruginosa* quinolone signal molecule overcomes the cell density-dependency of the quorum sensing hierarchy, regulates rhl-dependent genes at the onset of stationary phase and can be produced in the absence of LasR, Mol. Microbiol., 50 (2003) 29-43.

[34] E.E. Mann, K.C. Rice, B.R. Boles, J.L. Endres, D. Ranjit, L. Chandramohan, L.H. Tsang, M.S. Smeltzer, A.R. Horswill, K.W. Bayles, Modulation of eDNA Release and Degradation Affects *Staphylococcus aureus* Biofilm Maturation, PLOS ONE, 4 (2009) e5822.

[35] M. Fletcher, The effects of proteins on bacterial attachment to polystyrene, J. Gen. Microbiol., 94 (1976) 400-404.

[36] A. Gomes, E. Fernandes, J.L.F.C. Lima, Fluorescence probes used for detection of reactive oxygen species, Journal of Biochemical and Biophysical Methods, 65 (2005) 45-80.

[37] A. Almaguer-Flores, P. Silva-Bermúdez, R. Galicia, S.E. Rodil, Bacterial adhesion on amorphous and crystalline metal oxide coatings, Materials Science and Engineering: C, 57 (2015) 88-99.

[38] K. Hashimoto, H. Irie, A. Fujishima, TiO_2 photocatalysis: a historical overview and future prospects, Japanese Journal of Applied Physics, 44 (2005) 8269.

[39] L. Boulos, M. Prévost, B. Barbeau, J. Coallier, R. Desjardins, LIVE/DEAD® BacLight™: application of a new rapid staining method for direct enumeration of viable and total bacteria in drinking water, Journal of Microbiological Methods, 37 (1999) 77-86.

[40] O.N. Mileyeva-Biebesheimer, A. Zaky, C.L. Gruden, Assessing the impact of titanium dioxide and zinc oxide nanoparticles on bacteria using a fluorescent-based cell membrane integrity assay, Environmental Engineering Science, 27 (2010) 329-335.

[41] X. Lin, J. Li, S. Ma, G. Liu, K. Yang, M. Tong, D. Lin, Toxicity of TiO_2 nanoparticles to *Escherichia coli*: effects of particle size, crystal phase and water chemistry, PLOS ONE, 9 (2014) e110247.

[42] H.C. Flemming, J. Wingender, The biofilm matrix, Nature Reviews Microbiology, 8 (2010) 623-633.

[43] E. Burton, N. Yakandawala, K. LoVetri, M.S. Madhyastha, A microplate spectrofluorometric assay for bacterial biofilms, Journal of Industrial Microbiology & Biotechnology, 34 (2007) 1-4.

[44] Y.L. Ong, A. Razatos, G. Georgiou, M.M. Sharma, Adhesion forces between *E. coli* bacteria and biomaterial surfaces, Langmuir, 15 (1999) 2719-2725.

[45] K. Hori, S. Matsumoto, Bacterial adhesion: From mechanism to control, Biochemical Engineering Journal, 48 (2010) 424-434.

[46] C.J. van Oss, Hydrophobicity and hydrophilicity of biosurfaces, Current Opinion in Colloid & Interface Science, 2 (1997) 503-512.

[47] B. Jalvo, J. Santiago-Morales, P. Romero, R. Guzman de Villoria, R. Rosal, Microbial colonisation of transparent glass-like carbon films triggered by a reversible radiation-induced hydrophobic to hydrophilic transition, RSC Advances, 6 (2016) 50278-50287.

[48] M. Katsikogianni, Y.F. Missirlis, Concise review of mechanisms of bacterial adhesion to biomaterials and of techniques used in estimating bacteria-material interactions, Journal of European Cells and Materials, 8 (2004) 37-57.

[49] E.J. Wolfrum, J. Huang, D.M. Blake, P.C. Maness, Z. Huang, J. Fiest, W.A. Jacoby, Photocatalytic oxidation of bacteria, bacterial and fungal spores, and model biofilm components to carbon dioxide on titanium dioxide-coated surfaces, Environ. Sci. Technol., 36 (2002) 3412-3419.

[50] Y. Cai, M. Strømme, Å. Melhus, H. Engqvist, K. Welch, Photocatalytic inactivation of biofilms on bioactive dental adhesives, Journal of Biomedical Materials Research Part B: Applied Biomaterials, 102 (2014) 62-67.

[51] C.R.N. Rao, T. Takashima, W.A. Bradley, T.Y. Lee, Near ultraviolet radiation at the earth's surface: measurements and model comparisons, Tellus B, 36 (1984) 286-293.

[52] M.M. Khan, S.A. Ansari, M.I. Amal, J. Lee, M.H. Cho, Highly visible light active Ag@TiO_2 nanocomposites synthesized using an electrochemically active biofilm: a novel biogenic approach, Nanoscale, 5 (2013) 4427-4435.

[53] S. Kalathil, M.M. Khan, J. Lee, M.H. Cho, Production of bioelectricity, bio-hydrogen, high value chemicals and bioinspired nanomaterials by electrochemically active biofilms, Biotechnology Advances, 31 (2013) 915-924.

[54] N. Musee, M. Thwala, N. Nota, The antibacterial effects of engineered nanomaterials: implications for wastewater treatment plants, Journal of Environmental Monitoring, 13 (2011) 1164-1183.

Supplementary Material

Antimicrobial and antibiofilm efficacy of self-cleaning surfaces functionalized by TiO$_2$ photocatalytic nanoparticles against *Staphylococcus aureus* and *Pseudomonas putida*

Blanca Jalvo[1], Marisol Faraldos[2,*], Ana Bahamonde[2], Roberto Rosal[1,*]

[1] Department of Chemical Engineering, University of Alcalá, E-28871 Alcalá de Henares, Madrid, Spain
[2] Instituto de Catálisis y Petroleoquímica, ICP-CSIC, Marie Curie 2, 28049 Madrid, Spain

* Corresponding authors: mfaraldos@icp.csic.es, roberto.rosal@uah.es

CONTENTS:

Experimental. Surface hydrophobicity derived from contact angle measurements.

Figure S1. Evolution of MB with irradiation time on TiO$_2$-coated filters and slides. (B refers to blank runs and 1 and 2 to replicates.)

Figure S2. FilmTracer SYPRO Ruby biofilm matrix staining of samples with and without TiO$_2$, C(+) and C(-) respectively and with and without irradiation, L(+) and L(-) respectively for filters and slides kept in contact with *P. putida* and *S. aureus* for 48 h in the dark at 37 °C.

Figure S3. SEM images of *P. putida* (A, B, E and F) and *S. aureus* (C, D, G and H) biofilms on TiO2 glass slides (A, B, C and D) and TiO2 fiber filters (E, F, G and H) after 48 h incubation and before irradiation (A, C, E and G) and after 2 h irradiation (B, D, F and H).

Experimental. Surface hydrophobicity derived from contact angle measurements.

The Lifshitz–van der Waals (LW), electron donor (−) and electron acceptor (+) components of the surface tension were estimated from CA values for water, glycerol and diiodomethane according to the following expression in which θ are the pure liquid contact angles [1]:

$$\left(1 + \cos\theta\right)\gamma_L = 2\left(\sqrt{\gamma_S^{LW}\gamma_L^{LW}} + \sqrt{\gamma_S^+\gamma_L^-} + \sqrt{\gamma_S^-\gamma_L^+}\right) \tag{1}$$

In this approach, the total surface free energy (γ_S) is the sum of the non-polar London-van der Waals component (γ_S^{LW}) and the acid-base component (γ_S^{AB}), which in turn comprises two non-additive parameters: the electron-acceptor (γ_S^+) and the electron-donor (γ_S^-) surface tension parameters:

$$\gamma_S = \gamma_S^{LW} + \gamma_S^{AB} = \gamma_S^{LW} + 2\sqrt{\gamma_S^+\gamma_S^-} \tag{2}$$

The three components of the solid free surface energy, γ_S^{LW}, γ_S^+ and γ_S^- are unknowns that can be solved by measuring the CA with three liquids taking into account that the components of the liquid free surface energy, γ_L^{LW}, γ_L^+ and γ_L^- for the probe liquids are available in the literature for a number of pure substances [2]. According to Van Oss, the total interfacial tension between the solid film and water, γ_S, can be expressed as follows [3]:

$$\gamma_{SL} = \left(\sqrt{\gamma_S^{LW}} - \sqrt{\gamma_L^{LW}}\right)^2 + 2\left(\sqrt{\gamma_S^+\gamma_S^-} + \sqrt{\gamma_L^+\gamma_L^-} - \sqrt{\gamma_S^+\gamma_L^-} - \sqrt{\gamma_L^+\gamma_S^-}\right) \tag{3}$$

The free energy of interaction between two identical condensed phases immersed gives a direct measure of their hydrophobicity and can be derived from γ_{SL}:
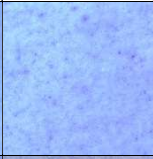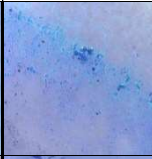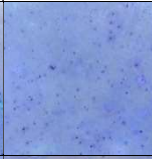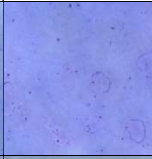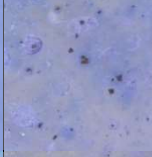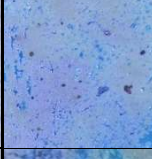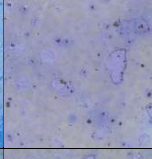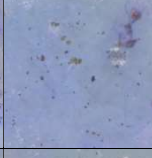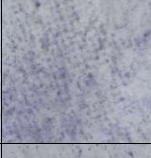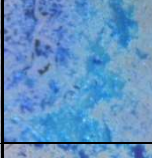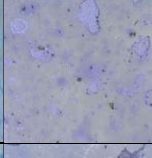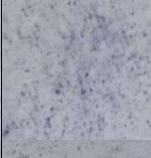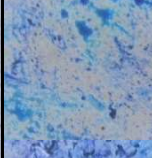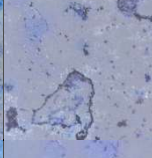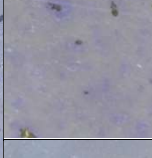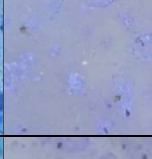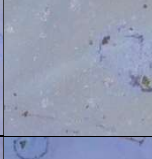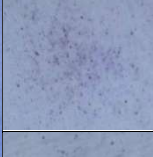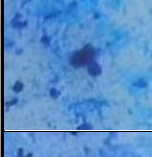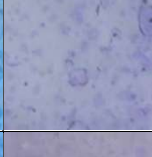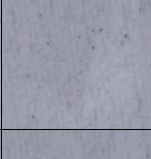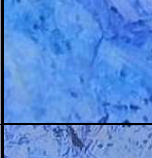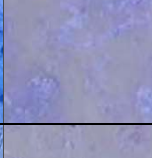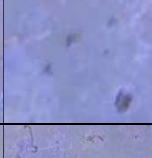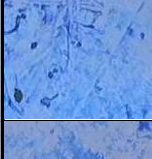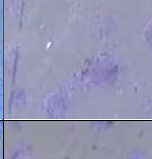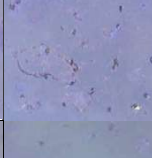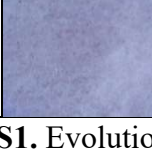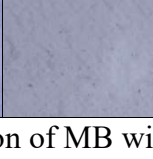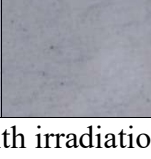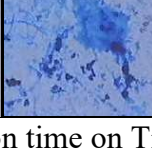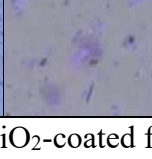
$$\Delta G_{SLS} = -2\gamma_{SL} \tag{4}$$

ΔG_{SLS} gives a measure of the hydrophobicity or hydrophilicity of the surface. If $\Delta G_{SLS} > 0$, the surface is hydrophilic, and if $\Delta G_{SLS} < 0$, it is hydrophobic.

[1] C.J. Van Oss, M.K. Chaudhury, R.J. Good, Interfacial Lifshitz-van der Waals and polar interactions in macroscopic systems, Chem. Rev., 88 (1988) 927-941.
[2] A. Holländer, On the selection of test liquids for the evaluation of acid-base properties of solid surfaces by contact angle goniometry. J. Colloid Interface Sci., 169 (1995) 493-496.

[3] C.J. van Oss, Development and applications of the interfacial tension between water and organic or biological surfaces, Colloids Surf B: Biointerfaces, 54 (2007) 2-9.

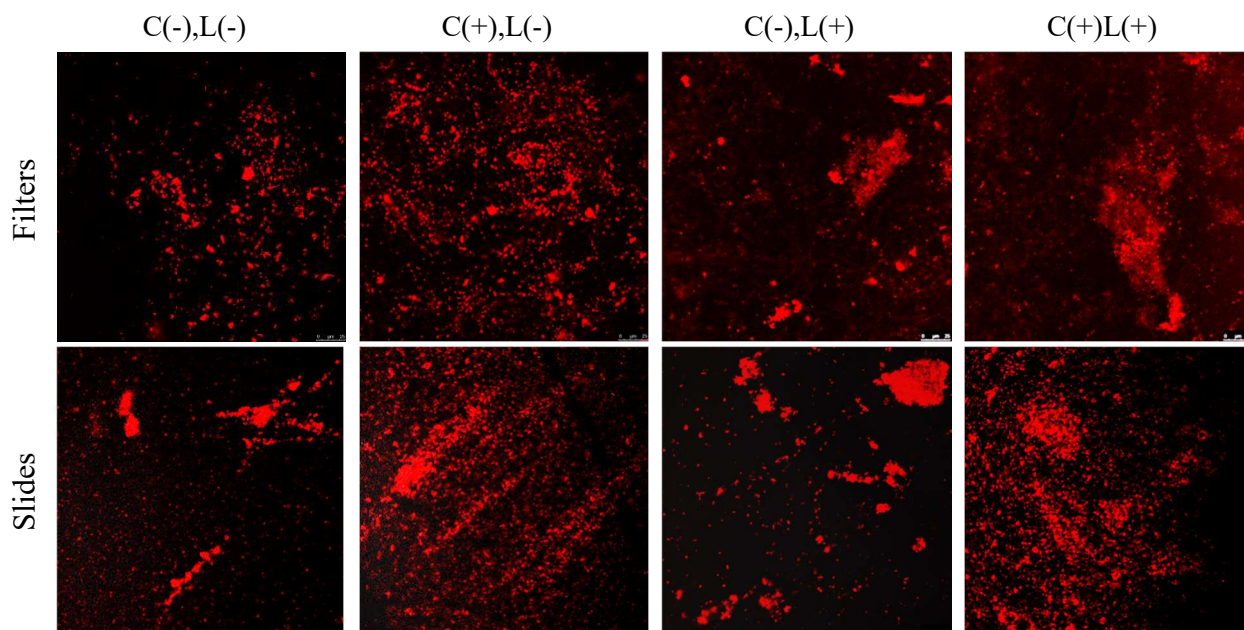|	Filters			Slides		
t (min)	B	1	2	B	1	2
0						
15						
30						
90						
180						
240						
300						
390						
480						
630						
750						

Figure. S1. Evolution of MB with irradiation time on TiO$_2$-coated filters and slides. (B refers to blank runs and 1 and 2 to replicates.)
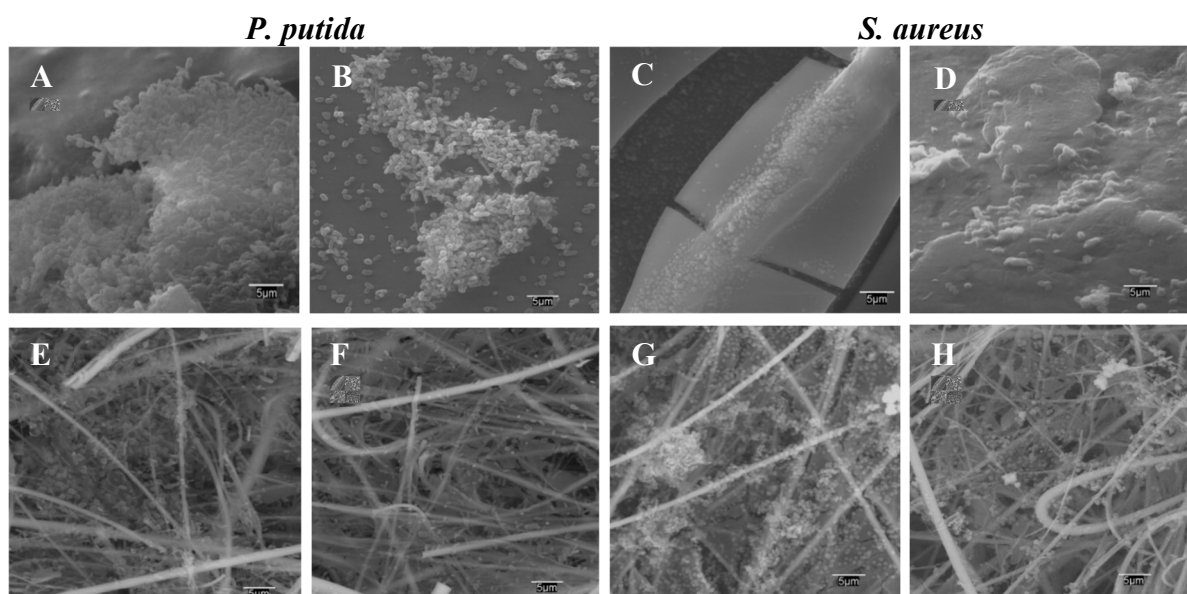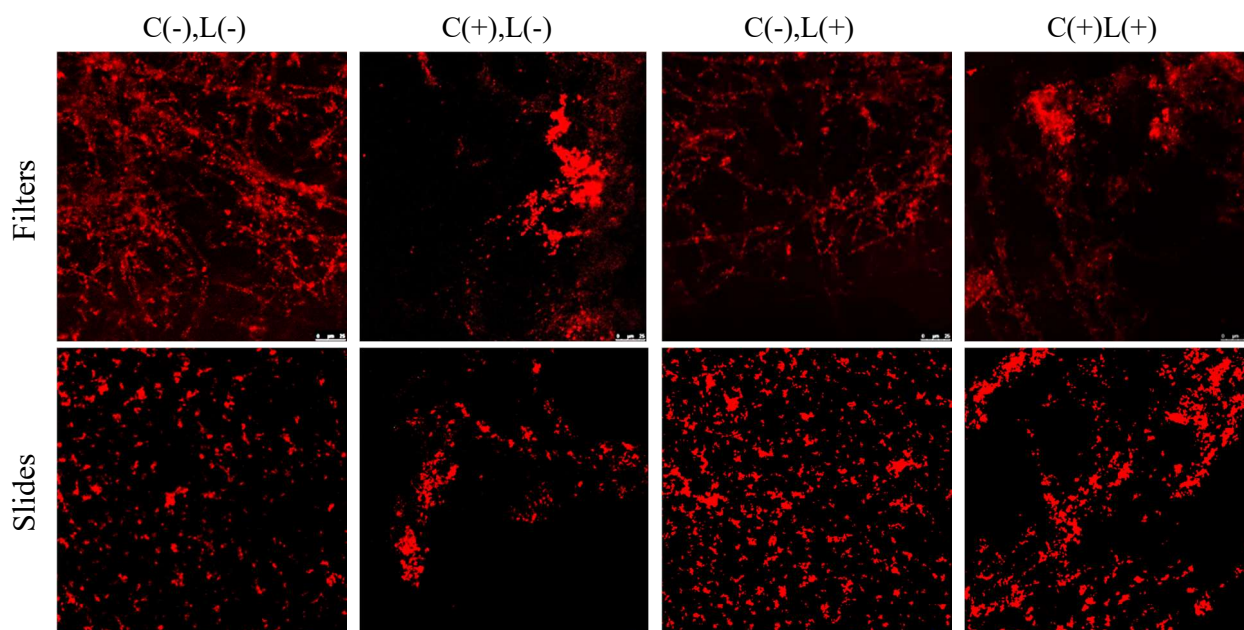
P. putida

S. aureus

Figure S2. SEM images of *P. putida* (A, B, E and F) and *S. aureus* (C, D, G and H) biofilms on TiO2 glass slides (A, B, C and D) and TiO2 fiber filters (E, F, G and H) after 48 h incubation and before irradiation (A, C, E and G) and after 2 h irradiation (B, D, F and H).

P. putida:

S. aureus:

Figure S3. FilmTracer SYPRO Ruby biofilm matrix staining of samples with and without TiO$_2$, C(+) and C(-) respectively and with and without irradiation, L(+) and L(-) respectively for filters and slides kept in contact with *P. putida* and *S. aureus* for 48 h in the dark at 37 °C.